

# On the binarity of Herbig Ae/Be stars

Deborah Baines<sup>1,2</sup>, René D. Oudmaijer<sup>2</sup>, John M. Porter<sup>3,†\*</sup>, Monica Pozzo<sup>4</sup>

<sup>1</sup> *U.K. Gemini Support Group, Dept. of Astrophysics, Oxford University, Keble Road, Oxford OX1 3RH, UK*

<sup>2</sup> *School of Physics and Astronomy, EC Stoner Building, University of Leeds, Leeds LS2 9JT, UK*

<sup>3</sup> *Astrophysics Research Institute, Liverpool John Moores University, Twelve Quays House, Egerton Wharf, Birkenhead CH41 1LD, UK*

<sup>4</sup> *Astrophysics Group, Imperial College London, Blackett Laboratory, Prince Consort Road, London, SW7 2AZ, UK*

Accepted –. Received –; in original form –

## ABSTRACT

We present high resolution spectro-astrometry of a sample of 28 Herbig Ae/Be and 3 F-type pre-main sequence stars. The spectro-astrometry, which is essentially the study of unresolved features in long-slit spectra, is shown from both empirical and simulated data to be capable of detecting binary companions that are fainter by up to 6 magnitudes at separations larger than  $\sim 0.1$  arcsec. The nine targets that were previously known to be a binary are all detected. In addition, we report the discovery of 6 new binaries and present 5 further possible binaries. The resulting binary fraction is  $68 \pm 11\%$ . This overall binary fraction is the largest reported for any observed sample of Herbig Ae/Be stars, presumably because of the exquisite sensitivity of spectro-astrometry for detecting binary systems. The data hint that the binary frequency of the Herbig Be stars is larger than for the Herbig Ae stars. The appendix presents model simulations to assess the capabilities of spectro-astrometry and reinforces the empirical findings. Most spectro-astrometric signatures in this sample of Herbig Ae/Be stars can be explained by the presence of a binary system. Two objects, HD 87643 and Z CMa, display evidence for asymmetric outflows. Finally, the position angles of the binary systems have been compared with available orientations of the circumprimary disc and these appear to be co-planar. The alignment between the circumprimary discs and the binary systems strongly suggests that the formation of binaries with intermediate mass primaries is due to fragmentation as the alternative, stellar capture, does not naturally predict aligned discs. The alignment extends to the most massive B-type stars in our sample. This leads us to conclude that formation mechanisms that do result in massive stars, but predict random angles between the binaries and the circumprimary disks, such as stellar collisions, are also ruled out for the same reason.

**Key words:** stars: pre-main sequence, techniques: spectroscopic, stars: binaries

## 1 INTRODUCTION

In contrast to the low mass stars, which are commonly accepted to form due to the gravitational collapse of a dusty cloud and the subsequent magnetically controlled accretion via a disc (e.g. Bertout 1989), the formation of the most massive stars is still very much uncertain. Part of this is due to the extreme rarity of these objects and the fact that they are very embedded in their molecular clouds, rendering them obscured. To make headway, it is important to study the optically visible Herbig Ae/Be stars as these have masses intermediate between the two above cases. The Herbig Ae/Be stars are now also found to mark the transition between the different formation mechanisms of low and high mass stars.

Recent studies indicate that the Herbig Ae stars present similar phenomena as T Tauri stars (Vink et al. 2003, 2005, see also Hubrig, Schöller & Yudin 2004), whereas the Herbig Be stars are similar to the more embedded Massive Young Stellar Objects (MYSOs, e.g. Drew et al. 1997).

To learn more about their formation, it is necessary to probe the (circum-)stellar environments of Herbig Ae/Be stars at the small scales where many important features for the further evolution such as discs, outflows, and binaries are found. Millimetre observations have detected discs in the size range of  $\sim 200$  to 3000 AU around Herbig Ae/Be stars (Mannings & Sargent, 1997 & 2000; Piétu, Dutrey & Kahané 2003), while near-IR coronagraphic observations of the Herbig Ae star HD 150193 (Fukagawa et al., 2003) and the Herbig Be star HD 100546 (Grady et al., 2001) reveal discs extending to  $\sim 190$  and 515 AU respectively. Using spectropolarimetry, Oudmaijer & Drew (1999) and Vink et al.

\* It is with great sadness that we have to report that, when this paper was in its final stages, John Porter suddenly died.

(2002) found evidence for even smaller scale discs, with sizes of the order of several stellar radii, around Herbig Ae/Be stars.

Pre-main sequence binary fractions have been determined from IR imaging (Bouvier & Corporon, 2001; Leinert, Richichi & Haas 1997; Pirzkal, Spillar & Dyck 1997; and Li et al., 1994) and optical spectroscopy (Corporon & Lagrange, 1999). These studies are based on limited samples of Herbig Ae/Be stars, but from extrapolations of the detections, the inferred binary frequency is almost double that of solar type Main Sequence stars for the period range probed (Leinert et al. 1997), and of the same order as the T Tauri stars (Köhler & Leinert, 1998).

In this paper we apply the technique of spectro-astrometry to study Herbig Ae/Be stars. This method is particularly suited to detect binary companions of emission line stars, and as we will show, can detect secondaries as much as 6 magnitudes fainter than the primary. As such it is among the most powerful methods to investigate binary frequencies, while it has the potential to probe even closer to the star and detect small scale structures in the circumstellar material.

The basic principle of spectro-astrometry is to measure the relative spatial position of spectral features from a longslit spectrum (Bailey, 1998). This is achieved by obtaining high spectral resolution long-slit spectra of an object and determining the centre of the point spread function (PSF) at each wavelength. In his pioneering paper, Bailey (1998) already illustrated that spectro-astrometry is effective at finding binaries and outflow structures around Herbig Ae/Be stars, focusing on the strong  $H\alpha$  emission of these objects. Later studies have found outflows and binary signatures from a sample of T Tauri stars (e.g. Takami, Bailey & Chrysostomou 2003 and references therein) and an outflow from a Brown Dwarf (Whelan et al. 2005).

Returning to the detection of binary stars, a system where only one of the components emits  $H\alpha$  displays a simple and easily detectable signature in the photo-centre of the spectrum. As the spatial profile is the sum of both stars, the peak is not located at the position of either star, but somewhere between the components, depending on the intensity ratio - analogous to the centre of motion of binaries. Because the  $H\alpha$  line intensity ratio changes across the line, the peak position shifts towards the  $H\alpha$  dominant star and the binary is revealed by an excursion in the positional spectrum. We also expect to see a decrease in the full-width-at-half-maximum (FWHM) of the spatial profile across  $H\alpha$  as it is dominated by only one star. This paper is the first to present and use this additional information that can be straightforwardly retrieved from the data. We will demonstrate later that the FWHM spectra have a strong diagnostic potential in assessing the properties of the objects under investigation.

In principle the method can be applied across any spectral line in which the intensity ratios of the two stars change from the continuum ratio; in the case of an absorption line the peak position will move away from the star displaying the absorption. Previously we reported on data of the pre-main sequence binary HK Ori (Baines et al. 2004), the aim of the present work is to further develop the technique and apply it to a large sample of Herbig Ae/Be stars. We observed 28 young Herbig Ae/Be stars and 3 F-type pre-main sequence stars spectro-astrometrically. The observations are

centred on  $H\alpha$  because the  $H\alpha$  emission line is usually by far the strongest feature in the spectrum of these objects. It is therefore particularly suitable to study the geometry of the circumstellar material, or as in this paper, binarity.

In Section 2 we describe the observations and the targets. The method used to extract information from such data is outlined here. Section 3 contains our results, which is followed by a discussion on our findings in Section 4. Section 5 summarizes the main conclusions and in the Appendix we discuss the strengths and limits of spectro-astrometry by simulating data.

## 2 OBSERVATIONS AND DATA REDUCTION

The data presented here are due to two observing runs, one in the southern and one in the northern hemisphere. The Herbig Ae/Be stars were selected from “Table 1” in the catalogue of Thé, de Winter & Perez (1994). All targets were chosen to be bright enough to obtain high S/N ratios in reasonable exposure times, and no previous knowledge of known binarity or otherwise was taken into account for the selection of the stars. Three objects, V380 Ori, Z CMa and HD 97048, that were observed by Bailey (1998) using spectro-astrometry were included to allow a consistency check. As a significant subset from Thé et al.’s catalogue was observed, the final sample is a representative selection of the intermediate mass pre-main sequence Herbig Ae/Be stars. Thirty-one objects were observed, 15 have B spectral type, 13 have spectral type A, while the remaining 3 objects are of F type. The log of the observations is shown in Table 1.

Observations were carried out on the 28th and 29th of January 2002 at the 3.9 m Anglo-Australian Telescope (AAT) using the RGO spectrograph with its 82 cm camera and a MITLL 2048 x 4096 CCD. The set-up gave a spatial pixel size of 0.15 arcsec, providing very good sampling of the seeing, which ranged from  $\sim 1.2$  to 2.6 arcsec. A 1200 line  $\text{mm}^{-1}$  grating was used to give a wavelength coverage of  $\sim 6300$  to 6800 Å. A 1 arcsec slit width resulted in a spectral resolution of about 40  $\text{kms}^{-1}$  at  $H\alpha$  sampled with  $\sim 0.15$  Å pixels. The spectra were obtained at four slit position angles (PAs, at  $0^\circ$ ,  $90^\circ$ ,  $180^\circ$ , and  $270^\circ$ ) for each object. This is to ensure optimal correction for any systematic effects such as curvature or optical distortion introduced by the spectrograph or a misalignment of the spectrum with the CCD columns. Wavelength calibrations were made from observations of a CuAr lamp.

Further observations were carried out from the 19th to the 23rd of September 2002 at the 2.5 m Isaac Newton Telescope, located at the Roque de Los Muchachos Observatory, La Palma, Spain. The IDS spectrograph with its 50 cm camera and an EEV10 2048 x 4096 CCD was used, giving a spatial pixel size of 0.19 arcsec. The seeing varied between  $\sim 1.3$  to 2.5 arcsec. The atmospheric conditions were worse during the early hours of 22nd September due to the presence of cirrus. An 1800 line  $\text{mm}^{-1}$  grating was used to give the same wavelength coverage as the AAT set-up, above. The 1 arcsec slit width resulted in a resolution of  $\sim 20$   $\text{kms}^{-1}$  at  $H\alpha$  (sampled with  $\sim 0.13$  Å pixel $^{-1}$ ). The spectra were obtained, as at the AAT, at four slit PAs ( $0^\circ$ ,  $90^\circ$ ,  $180^\circ$ , and  $270^\circ$ ) for each object, followed with an arc spectrum of a CuNe lamp.

**Table 1.** Log of the observations. Columns 2 to 4 list the RA, Dec and spectral type of the objects respectively. The  $V$  magnitudes in column 5 are taken from SIMBAD. Column 6 lists the dates of the observations and column 7 the exposure times. The average seeing for each object is given in column 8 and the number of photons per pixel in the stellar continuum in column 9. The  $1\sigma$  detection limit of both the position spectra and FWHM spectra are given in columns 10 and 11 respectively. These are the root-mean-square variations measured in line-free regions in the stellar continuum. Properties of the lines are listed in the final columns. The emission line profiles are classified as doublepeaked (D), singly peaked (S) or as showing (inverse) P Cygni (P) profiles. The equivalent width, with estimated errors of 10%, is also listed. References: for the spectral types: 1. Mora et. al. (2001), 2. SIMBAD, 3. Thé et. al. (1994).

| Object    | RA<br>(2000) | DEC<br>(2000) | Spec.<br>type           | $V$  | Date     | $t_{exp}$<br>(s) | Seeing<br>(arcsec) | Photons<br>( $\times 10^4$ ) | $rms_{pos}$<br>(mas) | $rms_{FWHM}$<br>(mas) | H $\alpha$ $W_\lambda$<br>( $\text{\AA}$ ) | H $\alpha$<br>Profile |
|-----------|--------------|---------------|-------------------------|------|----------|------------------|--------------------|------------------------------|----------------------|-----------------------|--|-----------------------|
| XY Per    | 03 49 36.3   | +38 58 55.5   | A2II <sup>2</sup>       | 9.4  | 21-09-02 | 6 x 3000         | 2.2                | 6.7                          | 2.0                  | 4.3                   | -6.6                                       | D                     |
| "         | "            | "             | "                       | "    | 23-09-02 | 8 x 900          | 2.1                | 6.1                          | 4.6                  | 21.0                  | -4.5                                       | D                     |
| AB Aur    | 04 55 45.8   | +30 33 04.3   | A0 <sup>2</sup>         | 7.1  | 29-01-02 | 4 x 180          | 2.4                | 16.0                         | 2.5                  | 4.5                   | -45  | P                     |
| "         | "            | "             | "                       | "    | 19-09-02 | 8 x 510          | 1.8                | 32.0                         | 0.9                  | 1.7                   | -21  | P                     |
| HD 31648  | 04 58 46.3   | +29 50 37.0   | A5v <sup>1</sup>        | 7.7  | 29-01-02 | 4 x 300          | 2.6                | 16.5                         | 2.3                  | 5.0                   | -17  | D                     |
| "         | "            | "             | "                       | "    | 19-09-02 | 4 x 1440         | 1.6                | 27.0                         | 1.1                  | 2.7                   | -14  | D/P                   |
| HK Ori    | 05 31 28.0   | +12 09 10.3   | A4/G1v <sup>1</sup>     | 11.9 | 29-01-02 | 8 x 300          | 2.4                | 1.6                          | 7.7                  | 19.2                  | -47  | D                     |
| HD 244604 | 05 31 57.3   | +11 17 41     | A3 <sup>2</sup>         | 9.4  | 28-01-02 | 4 x 600          | 1.9                | 10.5                         | 2.1                  | 4.5                   | -1.7                                       | D                     |
| T Ori     | 05 35 50.4   | -05 28 35     | A3iv <sup>1</sup>       | 9.5  | 28-01-02 | 4 x 600          | 1.6                | 6.7                          | 2.1                  | 5.3                   | -8   | D                     |
| "         | "            | "             | "                       | "    | 29-01-02 | 4 x 600          | 2.0                | 4.9                          | 2.6                  | 6.5                   | -8   | D                     |
| CQ Tau    | 05 35 58.5   | +24 44 54.1   | F5iv <sup>1</sup>       | 10.7 | 23-09-02 | 4 x 2400         | 1.8                | 4.7                          | 3.4                  | 8.2                   | -1.6                                       | invP                  |
| V380 Ori  | 05 36 25.4   | -06 42 57.7   | A0 <sup>2</sup>         | 10.0 | 29-01-02 | 4 x 300          | 2.5                | 1.4                          | 8.3                  | 19.1                  | -80  | S/D                   |
| MWC 137   | 06 18 45.5   | +15 16 52.4   | B0 <sup>3</sup>         | 11.2 | 22-09-02 | 8 x 600          | 1.2                | 1.7                          | 2.3                  | 11.2                  | -370                                       | S                     |
| HD 45677  | 06 28 17.4   | -13 03 11.1   | B3 <sup>3</sup>         | 8.0  | 29-01-02 | 8 x 300          | 2.8                | 13.8                         | 2.8                  | 6.8                   | -57  | D                     |
| MWC 147   | 06 33 05.2   | +10 19 20.0   | B6 <sup>2</sup>         | 8.8  | 28-01-02 | 4 x 600          | 2.1                | 20.5                         | 1.7                  | 4.2                   | -56  | D                     |
| MWC 158   | 06 51 33.4   | -06 57 59.4   | B9 <sup>2</sup>         | 6.6  | 28-01-02 | 8 x 45           | 1.6                | 22.0                         | 1.3                  | 3.2                   | -71  | D                     |
| "         | "            | "             | "                       | "    | 20-09-02 | 24 x 120         | 1.4                | 36.0                         | 0.9                  | 1.7                   | -77  | D                     |
| GU CMa    | 07 01 49.5   | -11 18 03.3   | B2v <sup>2</sup>        | 6.6  | 28-01-02 | 4 x 300          | 1.6                | 85.0                         | 1.4                  | 1.7                   | -7   | D                     |
| Z CMa     | 07 03 43.2   | -11 33 06.2   | B5 <sup>3</sup>         | 9.9  | 28-01-02 | 4 x 600          | 1.8                | 11.0                         | 1.5                  | 4.7                   | -68  | D                     |
| MWC 166   | 07 04 25.5   | -10 27 15.7   | B0iv <sup>2</sup>       | 7.0  | 28-01-02 | 4 x 240          | 1.8                | 33.0                         | 1.1                  | 2.4                   | -1   | D                     |
| HD 58647  | 07 25 56.1   | -14 10 43.6   | B9iv <sup>2</sup>       | 6.8  | 29-01-02 | 4 x 180          | 2.6                | 23.5                         | 2.0                  | 5.3                   | -6.0                                       | D                     |
| HD 85567  | 09 50 28.5   | -60 58 03.0   | B5v <sup>3</sup>        | 8.6  | 29-01-02 | 4 x 450          | 2.1                | 16.5                         | 2.0                  | 4.8                   | -40  | S                     |
| HD 87643  | 10 04 30.3   | -58 39 52.1   | B2 <sup>2</sup>         | 8.9  | 28-01-02 | 8 x 120          | 1.2                | 10.0                         | 1.2                  | 3.0                   | -145                                       | P,D                   |
| HD 95881  | 11 01 57.6   | -71 30 48.4   | A1/2III/IV <sup>2</sup> | 8.3  | 29-01-02 | 4 x 300          | 1.9                | 15.0                         | 2.0                  | 3.9                   | -11.5                                      | D                     |
| HD 97048  | 11 08 03.3   | -77 39 17.5   | A0 <sup>2</sup>         | 8.5  | 28-01-02 | 4 x 450          | 1.7                | 22.7                         | 1.4                  | 3.0                   | -25  | S                     |
| HD 98922  | 11 22 31.7   | -53 22 11.5   | B9v <sup>2</sup>        | 6.8  | 29-01-02 | 4 x 120          | 1.8                | 24.7                         | 1.2                  | 3.2                   | -17.5                                      | P                     |
| HD 100546 | 11 33 25.4   | -70 11 41.2   | B9v <sup>2</sup>        | 6.7  | 28-01-02 | 4 x 60           | 1.4                | 15.3                         | 1.4                  | 3.0                   | -35  | S                     |
| HD 104237 | 12 00 05.1   | -78 11 34.6   | A4 <sup>3</sup>         | 6.6  | 29-01-02 | 4 x 120          | 2.0                | 25.4                         | 1.6                  | 3.6                   | -26  | D/P                   |
| HD 135344 | 15 15 48.4   | -37 09 16.0   | A0/F4v <sup>3</sup>     | 8.6  | 29-01-02 | 4 x 600          | 1.7                | 25.4                         | 1.3                  | 3.0                   | -6.5                                       | S/D                   |
| HD 142527 | 15 56 41.9   | -42 19 23.3   | F6III <sup>2</sup>      | 8.3  | 29-01-02 | 4 x 450          | 1.7                | 30.0                         | 1.2                  | 3.0                   | -5.8                                       | P                     |
| 51 Oph    | 17 31 25.0   | -23 57 45.5   | B9.5III <sup>1</sup>    | 4.8  | 29-01-02 | 4 x 30           | 2.0                | 28.0                         | 1.4                  | 3.5                   | +4   | D                     |
| HD 190073 | 20 03 02.5   | +05 44 16.7   | A2iv <sup>1</sup>       | 7.8  | 21-09-02 | 8 x 1250         | 2.0                | 30.0                         | 1.1                  | 2.7                   | -24  | P                     |
| MWC 361   | 21 01 36.9   | +68 09 47.8   | B2v <sup>2</sup>        | 7.4  | 19-09-02 | 16 x 500         | 1.3                | 49.0                         | 0.9                  | 1.9                   | -59  | D                     |
| BH Cep    | 22 01 42.9   | +69 44 36.5   | F5iv <sup>2</sup>       | 10.8 | 22-09-02 | 4 x 2700         | 1.5                | 3.6                          | 2.7                  | 7.0                   | 0.0  | D/T                   |
| SV Cep    | 22 21 33.3   | +73 40 18     | A0 <sup>2</sup>         | 10.1 | 22-09-02 | 4 x 1800         | 1.7                | 3.3                          | 3.8                  | 7.2                   | +1.2                                       | D                     |
| MWC 1080  | 23 17 26.1   | +60 50 43     | B0 <sup>2</sup>         | 11.6 | 23-09-02 | 4 x 2400         | 1.8                | 2.1                          | 4.5                  | 8.7                   | -140                                       | P/D                   |

**Table 2.** The previously known binaries, the newly discovered binaries and possible binaries. Columns 2 and 3 list the binary separations and position angles from the literature, where available. Columns 4, 5 and 6 denote the position offset and the position angle of the binary system and FWHM change over the H $\alpha$  profile from our spectro-astrometric data. Note that the positional shifts across the line will always be *smaller* than the true separation (see text). The “possible” binaries were classified as such because they only show binary signatures in the FWHM spectra. Superscripts for the literature values are the references: 1. Fu et al (1997); 2. Leinert et al (1997); 3. Corporon (1998); 4. Pirzkal et al (1997); 5. Ghez, Neugebauer & Matthews (1993); 6. ESA (1997).

| NAME                | Lit Sep<br>(arcsec)            | Lit PA<br>(deg)    | H $\alpha$ shift<br>(arcsec) | PA<br>(deg)     | $\Delta$ FWHM<br>(arcsec) |
|---------------------|--------------------------------|--------------------|------------------------------|-----------------|---------------------------|
| Known Binaries:     |                                |                    |                              |                 |                           |
| GU CMa              | 0.655 $\pm$ 0.007 <sup>1</sup> | 192.6 $\pm$ 0.5    | 0.132 $\pm$ 0.005            | 192.5 $\pm$ 0.2 | 0.14 $\pm$ 0.01           |
| HK Ori              | 0.34 $\pm$ 0.02 <sup>2</sup>   | 41.7 $\pm$ 0.5     | 0.11 $\pm$ 0.01              | 40 $\pm$ 1      | -                         |
| MWC 147             | 3.10 $\pm$ 0.05 <sup>3</sup>   | -                  | 0.007 $\pm$ 0.002            | 72 $\pm$ 3      | 0.03 $\pm$ 0.01           |
| MWC 166             | 0.648 $\pm$ 0.007 <sup>1</sup> | 298.2 $\pm$ 0.5    | 0.050 $\pm$ 0.002            | 287.0 $\pm$ 0.4 | 0.05 $\pm$ 0.01           |
| MWC 361             | 2.25 $\pm$ 0.24 <sup>4</sup>   | 164 $\pm$ 1        | 0.005 $\pm$ 0.001            | 5 $\pm$ 3       | 0.005 $\pm$ 0.003         |
| MWC 1080            | 0.76 $\pm$ 0.02 <sup>2</sup>   | 267 $\pm$ 1        | 0.272 $\pm$ 0.004            | 267.3 $\pm$ 0.3 | 0.27 $\pm$ 0.01           |
| XY Per              | 1.331 $\pm$ 0.010 <sup>6</sup> | 76.300 $\pm$ 0.001 | 0.242 $\pm$ 0.002            | 85.0 $\pm$ 0.3  | 0.28 $\pm$ 0.01           |
| ”                   | ”                              | ”                  | 0.335 $\pm$ 0.006            | 83.8 $\pm$ 0.3  | 0.25 $\pm$ 0.03           |
| V380 Ori            | 0.154 $\pm$ 0.002 <sup>2</sup> | 204.2 $\pm$ 0.9    | 0.04 $\pm$ 0.01              | 204 $\pm$ 3     | -                         |
| Z CMa               | 0.100 $\pm$ 0.007 <sup>2</sup> | 122.5 $\pm$ 0.2    | 0.041 $\pm$ 0.002            | -               | 0.06 $\pm$ 0.01           |
| New Binaries:       |                                |                    |                              |                 |                           |
| AB Aur              |                                |                    | 0.029 $\pm$ 0.003            | 163 $\pm$ 6     | 0.12 $\pm$ 0.01           |
| ”                   |                                |                    | 0.023 $\pm$ 0.001            | 129 $\pm$ 2     | 0.07 $\pm$ 0.01           |
| HD 45677            |                                |                    | 0.013 $\pm$ 0.004            | 150 $\pm$ 17    | 0.05 $\pm$ 0.01           |
| HD 58647            |                                |                    | 0.016 $\pm$ 0.003            | 115 $\pm$ 10    | 0.03 $\pm$ 0.01           |
| HD 85567            |                                |                    | 0.029 $\pm$ 0.003            | 1 $\pm$ 2       | 0.05 $\pm$ 0.01           |
| HD 98922            |                                |                    | 0.039 $\pm$ 0.002            | 0 $\pm$ 1       | 0.010 $\pm$ 0.005         |
| MWC 158             |                                |                    | 0.016 $\pm$ 0.002            | 30 $\pm$ 7      | 0.050 $\pm$ 0.005         |
| Possible Binaries : |                                |                    |                              |                 |                           |
| HD 95881            |                                |                    |                              |                 | 0.020 $\pm$ 0.006         |
| HD 104237           |                                |                    |                              |                 | 0.04 $\pm$ 0.01           |
| HD 142527           |                                |                    |                              |                 | 0.04 $\pm$ 0.01           |
| HD 190073           |                                |                    |                              |                 | 0.020 $\pm$ 0.007         |
| HD 244604           |                                |                    |                              |                 | 0.02 $\pm$ 0.01           |

The data were reduced using the IRAF package (<http://iraf.noao.edu>). High signal-to-noise flat fields were made by combining many exposures with the spectrograph illuminated by a tungsten lamp. After subtracting the bias level and dividing by a normalised flat field, the 2-dimensional spectrum was fitted by Gaussian profiles in the spatial direction at each wavelength step. Visual inspection of the data confirmed that Gaussians are a proper representation of the real profiles. This results in a so-called position spectrum and FWHM spectrum, which gives the centre of the emission and FWHM of the emission as a function of wavelength respectively. Four position and four FWHM spectra were obtained at the different position angles. Any instrumental effects are largely eliminated by averaging those with opposite position angles (0 $^\circ$ -180 $^\circ$ , or 90 $^\circ$ -270 $^\circ$ ). This then returns two position and two FWHM spectra, one in the North-South (NS) direction and the other in the East-West (EW) direction.

The root-mean-square variations which give a measure of the uncertainty in the positioning of the centroid and FWHM were on average 2.2 mas and 5.5 mas respectively. These values were measured in a seeing which varied from 1.2 to 2.8 arcsec, and signal-to-noise ratios in the continuum ranging from 120 to 920 (see Table 1). The theoretical

precision of the centroid position is better for smaller seeing and higher SNR (Bailey, 1998; Porter, Oudmaijer & Baines 2004), and can easily reach sub-pixel values.

As Bailey (1998) noted, artifacts in the position spectrum can arise when sharp unresolved lines are observed. He suggested that such features are caused by telescope tracking errors or a consequence of seeing. One of the ways to eliminate such instrumental artifacts is to observe the objects at four different position angles, any real features should appear as mirror images of each other when obtained with slit Pa’s 180 $^\circ$  apart, while instrumental effects only appear in one direction.

In reality, this only reduces the effects to a certain extent. This is especially the case when steep changes in the flux spectrum occur, and visual inspection of the data is necessary to assess the reality of any resulting features. This is an important issue because many of the target stars have a strong double peaked H $\alpha$  profile with a dramatic change in intensity from the double peaks to the central absorption dip. Although the central absorption dips themselves are resolved, they still produce the type of signature in the position spectrum described by Bailey. Similarly, any non-uniformity in pixel to pixel response can produce features which are no true signatures in the stellar spectra. Despite

careful flatfielding, there is a number of pixels where this effect has not been fully eliminated. Any spectra falling across these coordinates show the same displacement. All systematic effects that have been identified are indicated by dotted lines in the spectro-astrometric plots shown later.

### 3 RESULTS

Out of 31 targets, we detect spectro-astrometric excursions in more than 20. The effects can often be simply explained with the presence of a binary companion, the results are summarized in Table 2. In the following we will start discussing the known binaries in the sample. As we know their system parameters, they provide an important check on the method. We then discuss the new and possible binaries, while the 2 objects with evidence for asymmetric outflows are discussed separately.

#### 3.1 Binaries

We begin our description by presenting GU CMa and MWC 1080. These two objects illustrate different aspects in spectro-astrometric data of binary systems.

*GU CMa* : GU CMa is a B2v Herbig Ae/Be binary with a separation of  $0.655 \pm 0.007$  arcsec and a PA of  $192.6 \pm 0.5^\circ$  (Fu et al., 1997). The North-Eastern star dominates the optical light. Figure 1 displays the data of the star. Large positional displacements across H $\alpha$  towards the North and East are present, indicating that the optically dominant object also dominates the H $\alpha$  emission. The excursions are a lower limit to the true separation as in the continuum both stars contribute to the spectrum. The FWHM spectrum changes across the H $\alpha$  line, as expected for a binary with one component dominating the H $\alpha$  emission. The FWHM in the continuum measures the unresolved binary, and decreases across H $\alpha$  when only the H $\alpha$  emitting component is measured. From the excursion of the H $\alpha$  line we derive the position angle of the binary to be  $192.5 \pm 0.2^\circ$ . This is very close to the PA found by Fu et al (1997).

*MWC 1080* : A different effect is visible when we consider an object which displays an H $\alpha$  P Cygni profile. MWC 1080 is a B0 Herbig Ae/Be star and Leinert et al (1997) measured a separation of  $0.76 \pm 0.02$  arcsec and a PA =  $267 \pm 1^\circ$ . Fig. 1 shows the spectro-astrometric data. H $\alpha$  is extremely strong with a peak that is 25 times the continuum, and a deep P Cygni absorption. In contrast to GU CMa, the positional spectrum exhibits more than one feature. Across the H $\alpha$  emission there is a small displacement to the East, coinciding with a decrease in the FWHM. As discussed above, such displacements are expected from a binary system with H $\alpha$  emission from one of the components.

The different aspect of MWC 1080 is the large westwards displacement across the H $\alpha$  P Cygni *absorption*. This is accompanied by a large increase in the FWHM and can be straightforwardly explained by the binary nature of the system. The relative contribution of the secondary increases as the light from the H $\alpha$  emitting primary diminishes across the P Cygni absorption. The centroidal position shifts to the secondary, while the FWHM now measures both stars and increases. From the positional excursions, we measure a PA

of  $267.3 \pm 0.3^\circ$ , very close to that derived from the imaging data reported by Leinert et al. (1997).

GU CMa and MWC 1080 are good examples of the technique of spectro-astrometry. Both objects were observed in seeing between 1.5 and 2 arcsec, but despite the fact that their separations are much smaller than the seeing, they were clearly and unambiguously revealed as binary objects. The introduction of the FWHM spectrum proves to be particularly useful in assessing whether any positional displacements are due to the presence of a binary. The excursions towards the H $\alpha$  emitting star allowed us to derive the position angle of the binary system. The resulting values are extremely close to those measured from imaging.

We continue our discussion with the full sample of the known binaries (with existing data listed in Table 2), and then further discuss the sample as a whole.

##### 3.1.1 Known binaries

Nine of the observed targets were previously known to be binaries with a largest observed separation of 3.1 arcsec. Their data are presented in Figures 1 and 2 and their observed values are listed in Table 2.

HK Ori is extensively discussed in Baines et al. (2004) and is not shown here. V380 Ori was also observed by Bailey (1998), who found a PA =  $206.7 \pm 1.1^\circ$ , and a positional displacement of  $0.039 \pm 0.003$  arcsec to the North-East. Our results are consistent with Bailey (1998) and are an important check on the reliability of our data and the repeatability of the technique. The PA listed in Table 2 is measured over the part of the spectrum that shows an obvious binary signature. XY Per was observed on 2 consecutive nights. Although the H $\alpha$  profile varied on these two days, we only show the first spectrum. The PA derived from both dates is the same. Z CMa was also observed by Bailey (1998) and will be discussed later.

In general, all of these objects show the spectro-astrometric signatures of a binary system. As outlined in the Appendix, the multiple peaks in the position and FWHM spectra of XY Per can even be explained by both components in the binary emitting H $\alpha$ . In addition, for 7 of the binaries the position angles derived from the spectro-astrometry agree very well with the existing data (Table 2). The object for which the PA was not reproduced is one of two objects with by far the largest separations (MWC 361 with a separation of 2.25 arcsec), much greater than the slit width. It has the smallest positional shift in our sample, and we confirmed the reality of the signature. It is only due to the comparatively large seeing values that we detect its secondary at all. MWC 147 also has a large separation, and care has thus to be taken in interpreting its derived PA. The binary has magnitude difference of  $\Delta R = 6.82$  mag, but an unpublished PA (Corporon, 1998, PhD thesis, cited by Millan-Gabet, Schloerb & Traub 2001). The fact that this binary, which has a separation of 3.1 arcsec and an  $R$  magnitude difference of almost 7 mag, can still be detected reveals how sensitive spectro-astrometry is at detecting binaries.

The empirical lesson learnt here is that in the case of wide binaries, (conservatively defined here as having separations larger than half the slit size, i.e.  $> \sim 0.5$  arcsec) we must be careful with any interpretation from the calculated PA.

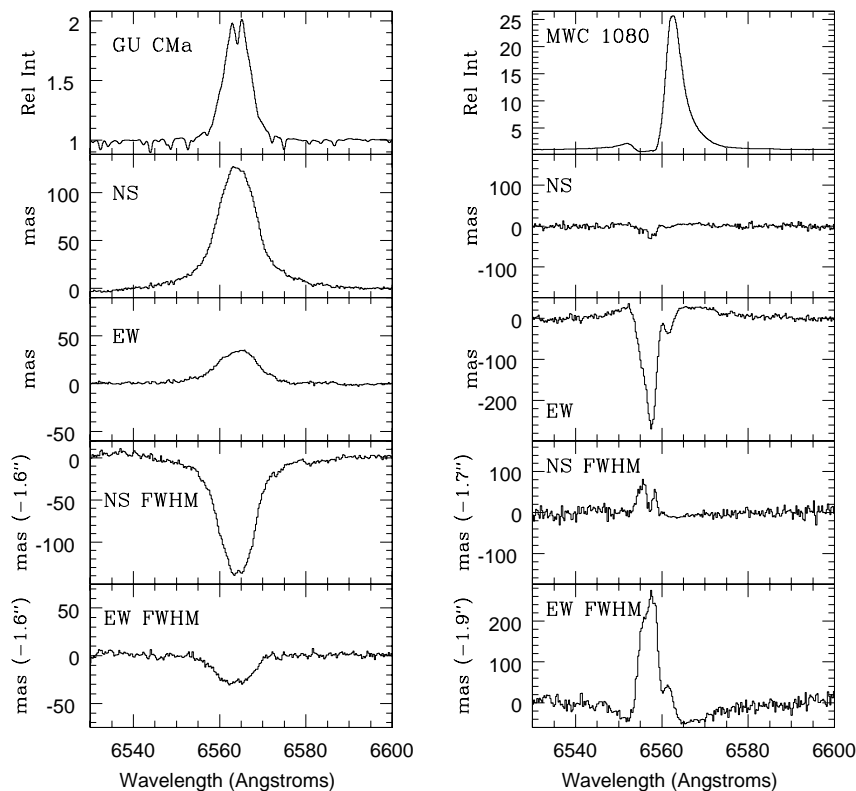


**Figure 1.** The spectro-astrometric plots of GU CMa (left) and MWC 1080 (right) centred on  $H\alpha$ . The graph shows, from top to bottom, the intensity spectrum, the centroid position of the spectrum in the North-South and East-West direction (with North and East up) and the FWHM of the spatial profiles of the NS and EW spectra respectively. For the FWHM spectra the vertical axis label includes the average seeing during the respective observations. Each position and FWHM spectrum has an arbitrary zero-point, which is adjusted to correspond to the continuum position and continuum FWHM position respectively.

Indeed, as noted by Porter et al. (2004), when the intent is to study binary systems and their secondaries, spectro-astrometric data has to be obtained with a very wide slit. The trade-off is a significant loss of spectral resolution.

Another important point to note is the observed change in FWHM across the  $H\alpha$  line. In Table 2 and Fig. 2, we find that the change is small for both small (HK Ori, V380 Ori) and large (MWC 147, MWC 361) separations and reaches a maximum in between. This can be understood in the following way. The large separation binaries become resolved in our data and the profile fitting routine will choose to fit the FWHM of only one component, across both the continuum and the line. In the case of small separations, the point spread functions of both components fall on top of each other and therefore result in only a small change in FWHM even if only one component is measured across the  $H\alpha$  line. Several variables come into play when interpreting the data and a first attempt to quantify the effects is presented in the Appendix. The empirical result that a significant drop in FWHM occurs when the binary separation is comparable to the slit size is confirmed by the simulations.

### 3.1.2 New binary systems

Within the dataset we find six stars which display a signature in the positional and FWHM spectra consistent with binarity of the objects (AB Aur, HD 45677, HD 58647, HD 85567, HD 98922, and MWC 158). According to our knowledge these are all new detections. Their data are presented in Fig. 3 and derived quantities are listed in Table 2. As all of the objects show obvious changes in the FWHM spectrum it follows from our finding outlined above and reinforced later, that the binary separations in all cases are greater than half the slit width ( $> 0.5$  arcsec). We can thus conclude that the companions of these wide systems are most likely at a separation of 0.5 to about 3.0 arcsec, the separation where the change in FWHM starts to decrease.

Both AB Aur and MWC 158 were observed during the two observing runs at different telescopes, and provide an internal consistency check. AB Aur qualitatively displays similar features on both occasions. This is important as it yields confidence in the reality of the detected features. However, the displacements are larger in January than in September, while the derived position angle is rather different (see Table 2). This is consistent with the idea that the binary has a larger separation than the slit width. Indeed, the seeing was slightly better in September, the light from the secondary therefore contributed less to the total spectrum. The result

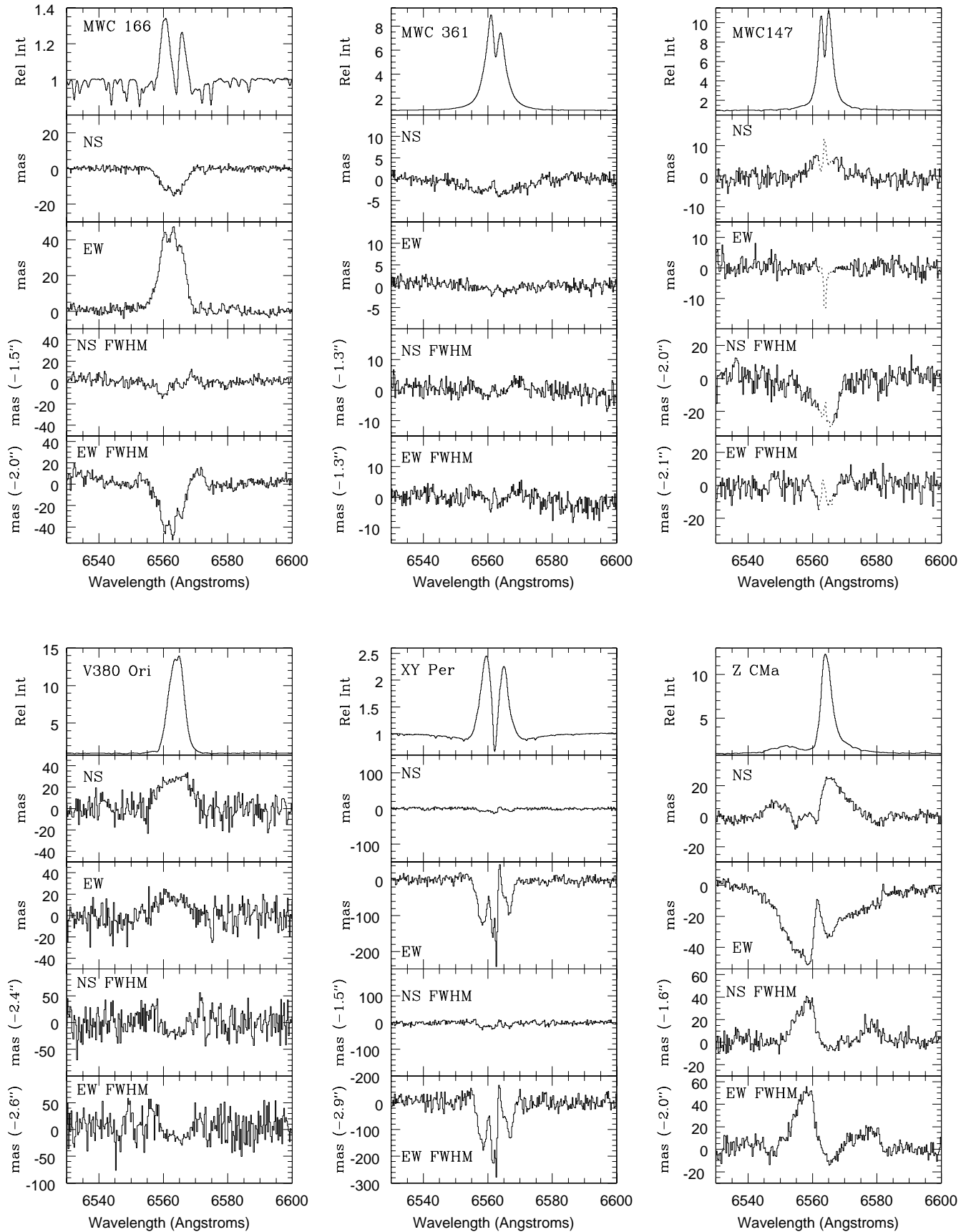


Figure 2. As the previous figure, but now for the remaining known binaries. Features that proved to be artifacts are indicated by a

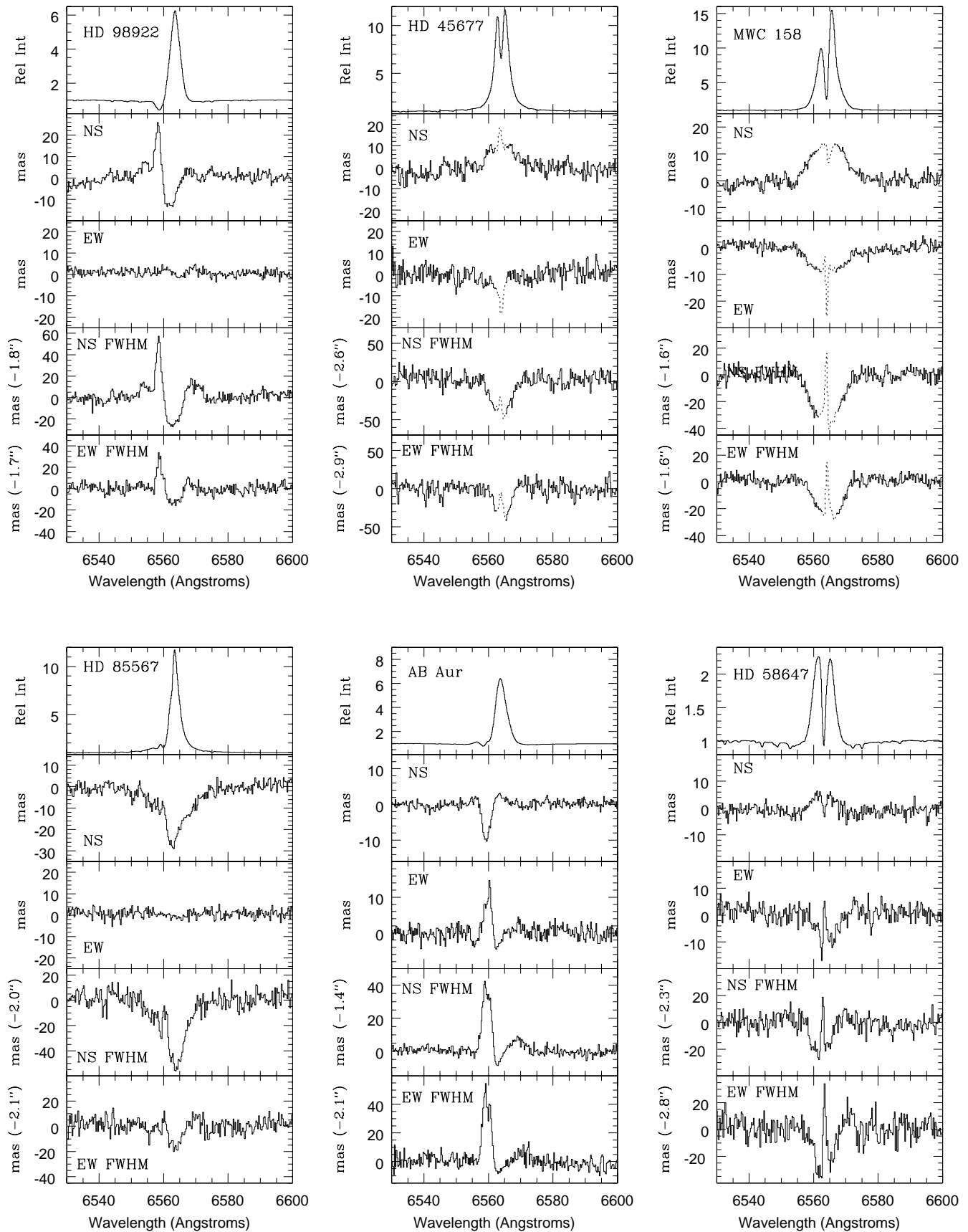
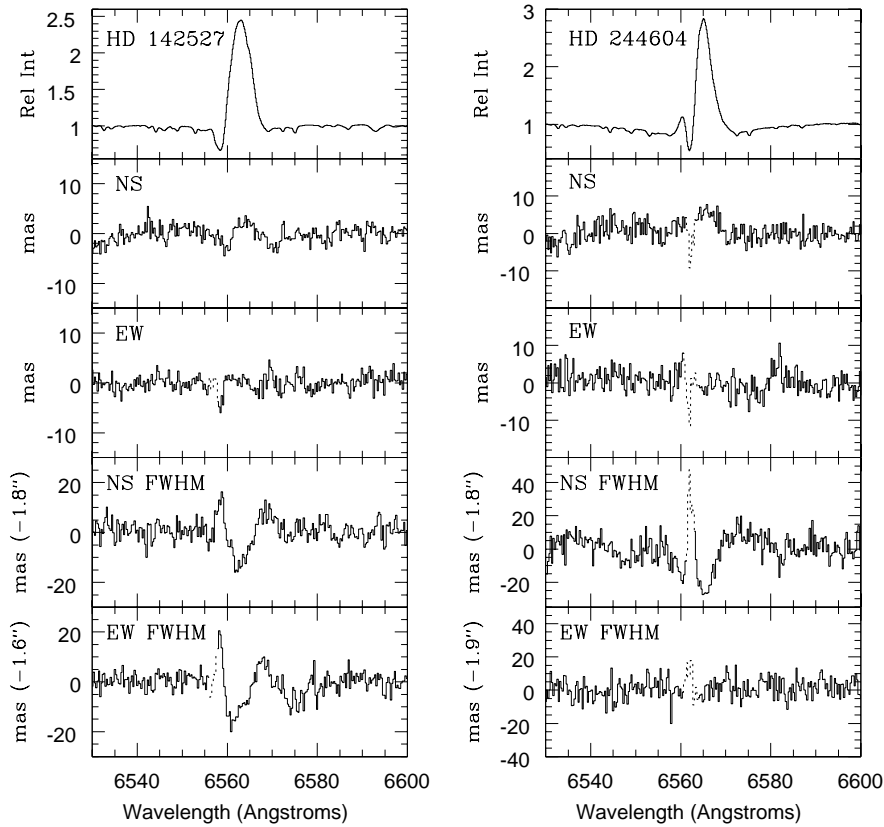
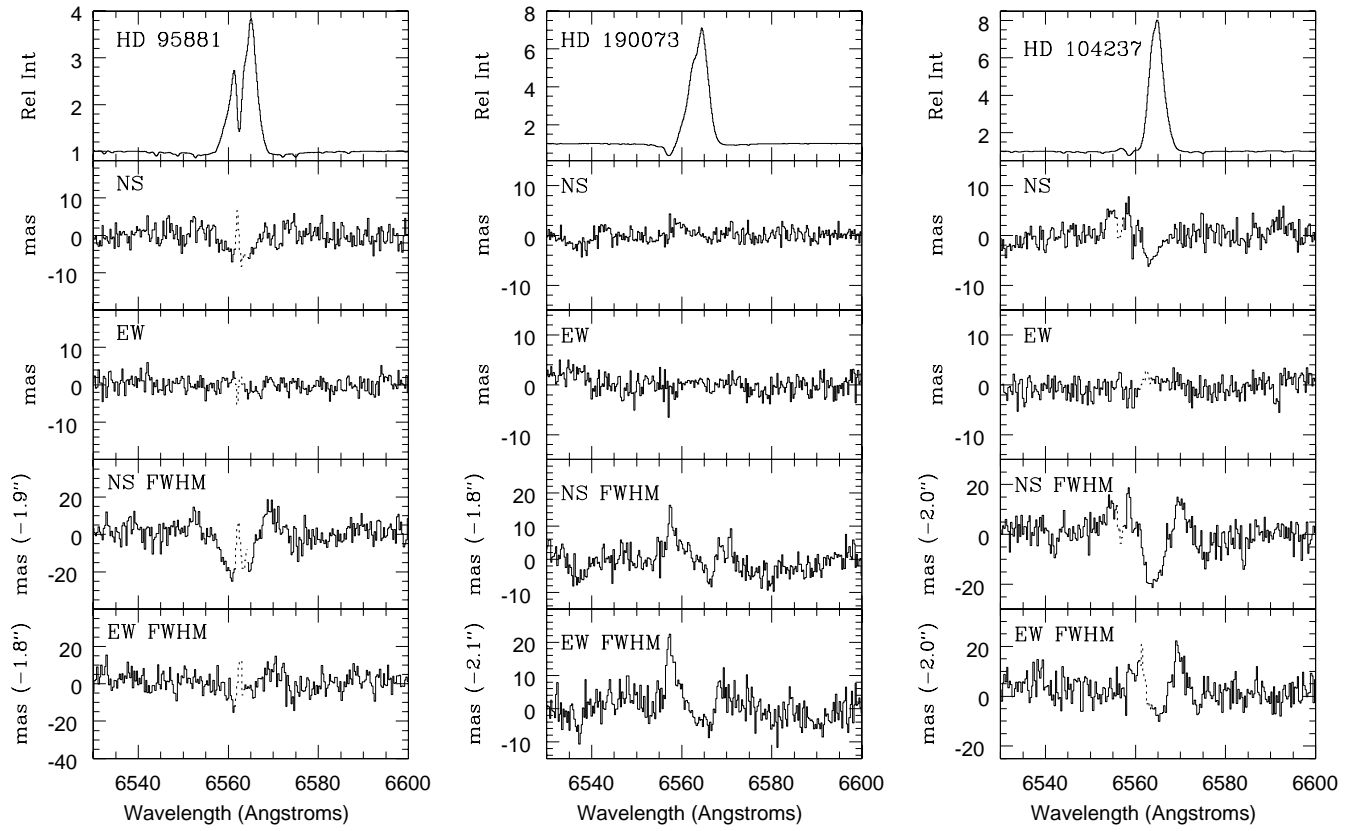


Figure 3. As the previous figure, but now for the new binaries.





**Figure 3.** Continued - Possible binaries

is that smaller excursions in the spectro-astrometric data occur, as observed. It also implies that the derived position angles from such binaries are highly uncertain.

An even more extreme effect occurred for MWC 158, whose binary signature in September all but disappeared. If it were not for the agreement of the AB Aur data and the other tests outlined earlier, it could be argued that the method is flawed. However, it is probable that in the better seeing the light from the secondary did not contribute enough to the total light to influence the spectro-astrometric data. In small seeing this effect is even stronger if the primary is not centered exactly in the centre of the slit.

We also wish to draw attention to HD 98922. This star is a known binary, but at a large separation of 7.8 arcsec, and a PA of  $343^\circ$  (Dommanget & Nys, 1994). If we assume that the primary is well centred, then its companion is located almost 2 arcsec outside the slit in the NS direction and about 7 arcsec in EW. As the seeing during the observations was 1.7 arcsec it is not impossible that we could just be detecting this binary in the North-South direction but it would be very difficult to detect the secondary in the East-West direction, especially in the FWHM spectrum. We therefore include this object in the list of new detections, rather than list it as a recovery of a known object.

### 3.1.3 Possible binary detections

Five stars within our sample show spectro-astrometric signatures that suggest a binary detection. These stars do not, or hardly, display any feature in the positional spectrum, but do show FWHM displacements consistent with a binary (HD 95881, HD 104237, HD 142527, HD 244604 and HD 190073). As the evidence for a binary is only visible in the FWHM spectrum, we prefer to be conservative and list these detections as “possible” binaries. The fact that the FWHM data display a larger excursion than the position spectra, indicates that the separation of the possible binaries is larger than half the slit-width. No position angles could be derived for these objects as the excursions in the positional spectra can not be measured.

## 3.2 Objects with evidence for outflow

### 3.2.1 Z CMa

ZCMa was also observed by Bailey (1998) who found that the spectro-astrometry of the linewings traces the (known) binary while the jet emission in the line centre traces a well known outflow (see also Garcia Thiébaud & Bacon, 1999). Although the emission has changed with respect to his spectrum, the positional displacements we observe are similar to those found by Bailey (1998).

The data are represented in a so-called XY-plot in Fig. 4. This graph plots the excursions in the EW and NS direction against each other. The red-shifted emission follows the binary direction, and the derived PA corresponds to the binary PA of  $120^\circ$  (Koresko et al. 1991; Leinert et al 1997). The blueshifted part of the line is dominated by jet emission and causes the positional displacements to move off the binary line in the direction of the jet at a PA of  $240^\circ$  (Poetzel, Mundt & Ray 1989). The FWHM spectrum (Fig.

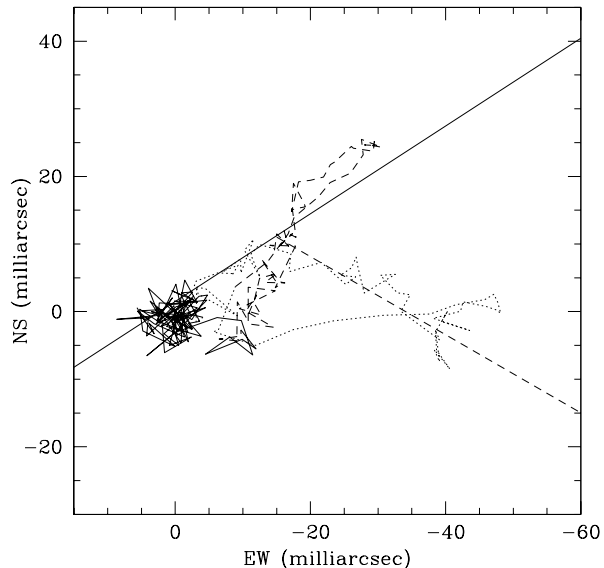


**Figure 4.** The spectro-astrometric XY plot of Z CMa, centred on  $H\alpha$ . The solid line shows the PA of the binary ( $122.5^\circ$ ), the dashed line shows the PA of the extended outflow ( $240^\circ$ ). Red and blueshifted components across the  $H\alpha$  profile are plotted as a dashed line and a dotted line respectively, to illustrate which of these are a result of the outflow, and which are a result of the binary. The blueshifted outflow is traced by the blueshifted positional displacements, except the far blue wing, which traces the binary. North is up and East to the left.

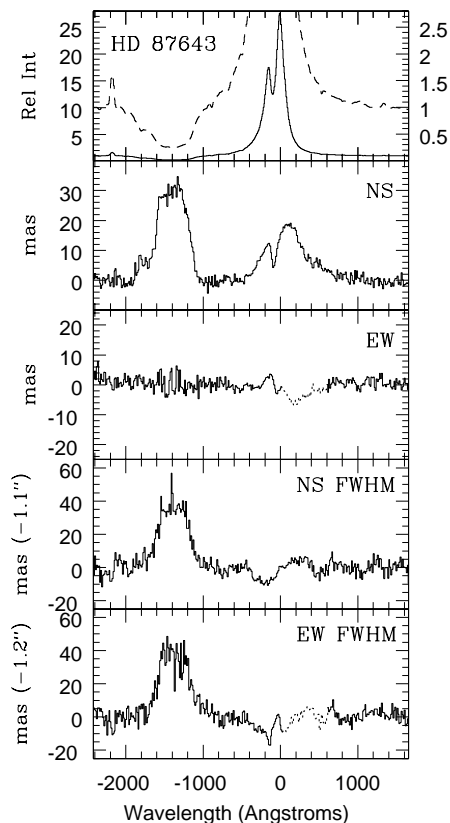
2) also indicates the presence of a binary; the redshifted displacements are consistent with the features being due to a binary as the FWHM decreases over the emission, and increases over the P Cygni absorption. There is an increase in the FWHM across the region dominated by the jet. From the direction of the binary displacement we can infer that the brightest infrared star also dominates the  $H\alpha$  emission.

### 3.2.2 HD 87643

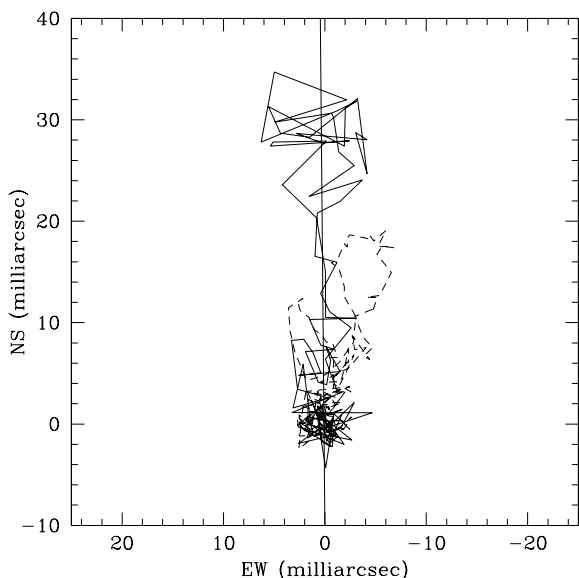
HD 87643 stands out in the complexity of its spectro-astrometry. Oudmaijer et al (1998) conducted an extensive study of the star by optical spectroscopy, spectropolarimetry and imaging. HD 87643 shows the B[e] phenomenon and also some characteristics typical for pre-main sequence stars. The spectropolarimetry revealed the presence of a rotating, expanding small scale ionized disc.

Figure 5 shows the spectro-astrometric plots of HD 87643. A northwards positional displacement across the P Cygni absorption is accompanied by a large increase in both the NS and EW FWHM spectra. There is no corresponding feature in the EW position spectrum however. Across the  $H\alpha$  emission line itself, a significant positional displacement northwards is present, but little change in the FWHM spectra. The XY plot is presented in Fig. 6 from 6520 to 6590  $\text{\AA}$ . This reveals that both the displacement across the P Cygni absorption (solid line) and emission (dashed) fall along the same PA of  $1.7 \pm 0.9^\circ$ .

The simplest scenario, a binary system, fails to explain the data. The NS position spectrum shows a displacement



**Figure 5.** The spectro-astrometric plots of HD 87643, centred on  $H\alpha$ . The dashed line in the top panel is a magnification of the spectrum, to illustrate the P Cygni absorption.



**Figure 6.** The XY plot of HD 87643 centred on  $H\alpha$ , between 6520 to 6590  $\text{\AA}$ . The displacement across the P Cygni absorption is shown as a solid line, and across the emission as a dashed line.

across the P Cygni absorption, as already described for some binaries earlier. However, in contrast to those cases, the positional displacement across the  $H\alpha$  emission is in the same direction as that of the absorption. This would imply that the secondary dominates the  $H\alpha$  emission, but the primary would have the P Cygni profile. Therefore, both primary and secondary would be emitting  $H\alpha$ . Although contrived, this situation is not impossible. However, in the EW direction the argument for a binary system breaks down. No positional displacement is observed across the P Cygni absorption, but the EW FWHM still increases across the P Cygni absorption - contrary to what is expected for a binary, and contrary even to what is observed in the NS direction.

A second scenario, is that the  $H\alpha$  emission is due to an outflow. An increase in both the NS and EW FWHM across the P Cygni absorption could be expected from an extended outflow. The absence of a positional displacement across a feature, in this case the P Cygni absorption in the EW, simply indicates that the outflow is symmetric and extended in that direction. At the same velocities within the P Cygni absorption, a displacement and an increase in FWHM is observed towards the North, indicating that this outflow is asymmetric in the NS direction. The  $H\alpha$  emission also shows a displacement towards the North, although not as large as in the absorption. No increase in the FWHM is seen across the  $H\alpha$  emission, and presumably this structure is closer to the star.

From these spectro-astrometric displacements we suggest that we are observing two different but aligned velocity outflows. Across the P Cygni absorption we detect a high velocity outflow, symmetric in the EW direction and asymmetric towards north. Closer to the star is an extended  $H\alpha$  emission region, also with an extra component towards the north.

Such high velocity positional displacements could be produced by a bow shock type structure towards the north. The low velocity positional displacements may be from the same outflow as the high velocity displacement, but closer to the star. The polarization of HD 87643 shows a disc-like structure surrounding the star with polarization angle of  $\sim 20^\circ$  and is probably viewed at a high inclination angle (Oudmaijer et al., 1998). Our results imply a high and low velocity outflow predominantly located towards the north ( $PA = 0^\circ$ ). This is closer to the PA of a polar outflow ( $\sim 20^\circ$ ) than the disc when assuming the disc lies perpendicular to the polarization. Finally, we note that the spectro-astrometric displacements of HD 87643 stand out as different to all our other Herbig Ae/Be stars, and hence HD 87643 may indeed belong to the B[e] supergiant group.

## 4 DISCUSSION

We have observed 28 Herbig Ae/Be stars and 3 F-type pre-main sequence stars using spectro-astrometry. The data prove both from an empirical point of view and from simulations described in the Appendix very powerful in discovering binary objects. The method exploits the fact that the components have different spectra and is used here across the  $H\alpha$  emission line. After a discussion on spectro-astrometry itself, we will investigate the implications of the large binary fraction of these intermediate mass pre-main sequence ob-

jects for their formation, and investigate the alignment of the binary systems with the circumprimary discs.

#### 4.1 Spectro-astrometry as a tool to investigate binary stars

As this paper presents the first comprehensive study into binarity using spectro-astrometry, we briefly discuss the possibilities and limitations of the method here.

##### 4.1.1 On the capabilities of spectro-astrometry

Checks on known binary systems that were present in our sample - which were all retrieved - and the repeat observations of objects at different telescopes indicate that the method is robust. The smallest separation binary that was observed has a separation of 0.1 arcsec. The technique can cope with a large flux difference, both simulations and observations (MWC 147) indicate that secondaries which are up to 6-7 magnitudes fainter can still be detected. The position angles of the binary systems can be reliably reproduced for separations smaller than the slit-width. For larger separations, only a fraction of the light from the secondary will fall within the slit. This may result in a smaller positional displacement than expected and an incorrect binary PA. We should stress that the position of the photo-centre only provides a lower limit to the true separation. This is because it measures the position of one star across the emission line, but a weighted average of the two stars in the continuum. The magnitude of the displacement depends on the seeing, separation and, crucially, flux-difference of the components.

The FWHM spectrum, which has never before been discussed in the literature, provides important additional information. It gives diagnostic clues about the nature of the position spectra. The stars with P Cygni profiles provided an illustrative example of the different types of behaviour that can occur when observing absorption or emission. The FWHM decreases over the emission, as only one object is visible. In contrast, the FWHM increases over the P Cygni absorption as the fainter secondary becomes more dominant in the spatial profile. In addition, the FWHM information also provides an important indication of the binary separation. Binaries with separations approximately larger than the slit width have FWHM displacements as large as, or larger than, the position offset.

To learn more about the capabilities of the method, simulations were performed and a selection of the results is presented in the Appendix. The simulations reinforce the empirical results. The lower limit to the binary separation is found to be smaller than the smallest separation binary discussed here, and is of order  $\sim 0.010$  arcsec, with a dependency on the observing conditions and binary parameters. Spectro-astrometry can detect secondaries up to 6 magnitudes fainter than the primary even for seeing values of  $\sim 1.5$  arcsec.

As the separation is an unknown, it is virtually impossible to know the flux losses induced by the limited slit width (see also Porter et al. 2004). It is therefore not feasible to retrieve separations from spectro-astrometric data without dedicated modelling while a large slit width is required to ensure all light from the secondary is captured. For the same

reason it is not possible to derive the spectrum of the secondary for wide binaries with confidence. This potentially important information for the understanding of binary formation needs dedicated observations as discussed by Porter et al. (2004).

##### 4.1.2 Detection of binary systems

Among the 28 Herbig Ae/Be stars observed, 15 binaries (6 of them new discoveries) have been detected. A further 4 Herbig Ae/Be and 1 F type object are considered possible detections of a binary. The spectro-astrometry is able to reveal the presence of a binary only if the respective spectra are different. In the present study we take advantage of the fact that one of the components dominates the H $\alpha$  emission.

Before we begin interpreting the data, let us first consider selection effects. The first and foremost question to ask is whether there is any relationship between the strength of the H $\alpha$  emission and the detection of a binary. By its very nature, the method is less efficient for those objects with small spectral differences and hence those objects with weak H $\alpha$  emission. Indeed, the 3 objects with positive H $\alpha$  equivalent widths, indicating very weak emission if at all, SV Cep (A-type), BH Cep (F-type), and 51 Oph (B-type) are not found to be a binary. For these objects it is reasonable to assume that the method would not have revealed a binary even if a companion were present. For the remainder of the sample, it would appear that the method is not biased against faint H $\alpha$  emitters. The next weakest H $\alpha$  emitter is MWC 166. Although its emission is only 40% above the continuum (Fig. 2), the binary is a clean detection. The strongest H $\alpha$  emitter (MWC 137) turns out to be a non-detection, while there is no obvious difference between the strength of detections and non-detections. We therefore conclude that the statistics are not significantly affected by the strength of the emission line.

Another issue is the signal-to-noise ratio of the data. The higher SNR spectra could in principle be more efficient at detecting signatures. The two objects with the worst SNR in the position spectra are HK Ori and V380 Ori but are both binary detections, while generally, both detections and non-detections have on average comparable SNR. As there is a narrow range in the rms variations in the photo-centre of the data (1-8 milli-arcseconds, with most below 3 mas, see Table 2) to first order the quality of the data has no obvious effect on the results.

## 4.2 On the binarity of Herbig Ae/Be stars

The observations return a Herbig Ae/Be binary frequency of  $54 \pm 11\%$  (68% confidence interval). The fraction rises to  $68 \pm 11\%$  if we include the possible detections. Recent studies of Herbig Ae/Be stars have observed binary frequencies of 25 - 40% (using IR imaging: Bouvier & Corporon, 2001; Leinert et al., 1997; Pirzkal et al., 1997; and Li et al., 1994; and using optical spectroscopy: Corporon & Lagrange, 1999).

The present study increases the *observed* fraction significantly, presumably because many of the previous studies have lower sensitivity to fainter companions, and does point toward even larger fractions when considering observational

biases. For example, Pirzkal et al (1997) found a binary frequency of 23% from a sample of 39 Herbig Ae/Be stars. Taking into account their observational biases they calculated that the binarity of Herbig Ae/Be stars should be  $\sim 85\%$ , and find this is comparable to that extrapolated for T Tauri stars (e.g. Ghez et al., 1993 find an uncorrected binary frequency of  $60\pm 17\%$ ), and exceeds that of near solar type Main Sequence stars (57%; Duquennoy & Mayor, 1991). These numbers compare well with the compilation of binary statistics for B main sequence stars by Abt, Gomez & Levy (1990), who found an average of 0.7 companions per primary and a binary frequency, as deduced from their tables, of 55%.

Finally, the high binary frequency observed in a sample such as the present one could be the result of observational bias. When dealing with a magnitude limited sample, one preferentially includes binaries as they would appear brighter than a single star of the same type. This bias is larger when the brightness contrast between both components is smaller. This could be investigated by spatially resolved imaging at optical wavelengths (yielding the light contrast directly) or dedicated spectro-astrometry, yielding not only the light contrast to be measured, but also allowing the splitting of the spectra, making it possible for the spectral types of the components, and ultimately the mass ratio, to be determined. Having said that, the Herbig Ae/Be star catalogue of Thé et al. (1994) is by the subjective nature of which it is compiled, subject to many biases, amongst which the brightness of the targets is perhaps the only one that can be quantitatively addressed.

#### 4.2.1 Binarity as function of spectral type

Let us now turn to the percentage of binaries within the Herbig Be stars and Herbig Ae stars.

Among the theories for binary star formation we find the stellar capture model in small ( $N < 10$ ) clusters, where the natural outcome is the larger binary fraction for more massive stars (e.g. McDonald & Clarke 1995). Multiple fragmentation models also predict a larger binary fraction with stellar mass. These consider the breaking up of a molecular cloud from which fragments, which become the binary components, can form. The fragmentation models predict a much higher binary fraction in general than the capture models. In contrast, the so-called  $N=2$  fragmentation models are different from the multiple fragmentation models in the sense that the binary frequency has no dependence on mass (see e.g. the review by Clarke 2001).

Taken at face value, more binaries were detected around the Herbig Be stars (11 out of 15;  $73^{+12}_{-16}\%$  - interestingly very close to Pirzkal's prediction) compared with the Herbig Ae stars (4 out of 13;  $31^{+18}_{-14}\%$ ). Of the 5 possible binary detections 4 have A spectral types and 1 has an F spectral type. This increases the Herbig Ae observed binary frequency to  $62^{+15}_{-17}\%$ .

The fact that the number of confirmed Herbig Be binaries is larger than that of the Herbig Ae binaries could point at a real effect. It could either mean that Herbig Be stars have a larger percentage of companions than Herbig Ae stars, or that the spectro-astrometry is more efficient at detecting companions around Herbig Be stars than Herbig

**Table 3.** The binaries that have a measurement of the PA of the circumprimary disc available. The third column shows the binary PA, taken from Table 2. Literature values are denoted with <sup>L</sup>. The fourth column shows the intrinsic polarization angle derived from spectropolarimetry by Vink et al. (2005), the values between brackets are quoted to be uncertain. The last column shows the difference (computed to be in the range  $0..90^\circ$ ) between the binary PA and the intrinsic polarization PA.

| NAME     | Sp Tp | PA<br>(deg) | $\Theta_{Pol}$<br>(deg) | $\Delta$<br>(deg) |
|----------|-------|-------------|-------------------------|-------------------|
| MWC 166  | B0    | $298^L$     | 50                      | 68                |
| MWC 361  | B2    | $164^L$     | (90)                    | 74                |
| XY Per   | A2    | $76^L$      | (70)                    | 6                 |
| HD 58647 | B9    | 115         | 20                      | 85                |
| MWC 158  | B9    | 30          | 135                     | 75                |
| HD 45677 | B     | 150         | 70                      | 80                |

Ae stars (which is reinforced by noting that all “possible” detections were of A or F type, but no B type).

From *K*-band imaging Testi et al (1997) found a correlation between the mass of Herbig Ae/Be stars and the number of *K*-band stars detected around it. From further observations of 44 young stars, covering almost uniformly the whole spectral range from O9 to A7, Testi, Palla & Natta (1999) conclude that rich clusters (with densities up to  $10^3 \text{ pc}^{-3}$ ) only appear around stars earlier than B5. If early B type stars are associated with dense clusters then one could assume that a higher percentage of Herbig Be stars will have companions. Bonnell & Clarke (1999) show that the observational data of Testi et al (1999) do not require such an interpretation, but are instead compatible with the statistics of randomly assembling stars from the initial mass function into clusters with a range of sizes. Therefore, a higher binary frequency observed around Herbig Be stars may not have implications on the initial formation of massive stars, but may have implications on the further evolution of Herbig Be stars. We note that the different statistics between the Herbig Ae and Herbig Be objects in this paper only become comparable when taking into account the possible detections.

#### 4.2.2 On the position angles of the binaries and the circumprimary discs

An additional question, already alluded to in the Introduction addresses not only the formation of binary stars, but also the formation of the most massive Herbig Be stars - for which stellar mergers have been proposed (see Bonnell, Bate & Zinnecker 1998). In the following we investigate whether the derived position angles from the binaries are of any help in this respect.

A prediction from the above mentioned models concerns the alignment of the binary systems and the (possibly accretion) discs around the primary stars. Capture models predict randomly oriented discs around both components of the binary, while fragmentation models predict co-planar discs around the stars. For the merger models to still result in a binary, we need a triple system to begin with. It is unlikely that the merger process will result in a disc aligned with the original tertiary component, hence random orienta-

tions would be expected, as also noted by Bally & Zinnecker (2005).

Wolf, Stecklum & Henning (2001) and Jensen et al. (2004) present studies of T Tauri stars and found the binary systems in their samples to be preferentially aligned with the discs, thus favouring the fragmentation model for low mass stars. A similar study was performed for Herbig Ae/Be stars by Maheswar, Manoj & Bhatt (2002), who find that many Herbig binaries are parallel or perpendicular to within  $30^\circ$  from the broad band polarization.

We have the sample in hand to improve this sort of studies and extend it to higher masses. To this end we draw on the spectropolarimetric results of Vink et al. (2002, 2005). Inspired by the seminal work by Poeckert & Marlborough (1976) who proved the existence of discs around Be stars with this method, they use the  $H\alpha$  line de-polarization to reveal the presence of small scale electron scattering discs around pre-main sequence stars. An advantage of this method is that the intrinsic angle of the polarization can be directly determined and is independent of the value of the interstellar polarization. The latter affects the previous broadband polarization studies (see e.g. the discussion by Jensen et al. 2004). For optically thin scattering, which is found to be the case for Herbig Ae/Be stars (Vink et al. 2005), the intrinsic polarization angle is perpendicular to the disc. As the polarization is due to electron-scattering, the discs are very small (of order stellar radii; Cassinelli, Nordsieck & Murison, 1987) and we can be confident that the polarization traces the disc around the *primary* object and not a circumbinary disc.

The sample of objects with a PA determination for both the binary and the disc measured from the spectropolarimetry contains 7 targets. From this we have to exclude AB Aur whose data on two occasions resulted in two different position angles indicating that the binary is too wide to believe the PA in the first place. We list the intrinsic polarization angles of the remaining stars in Table 3. The majority of the objects (5 out of 6) have an angle difference to within  $\approx 20^\circ$  of perpendicular, indicating that the circumprimary discs and binaries are well aligned. XY Per is the exception, with a difference of  $6^\circ$ .

To get a quantitative handle on this finding we computed the cumulative distribution functions of the data and several assumed distributions, and then calculated the Kolmogorov-Smirnov (KS) statistic. In Fig. 7 we show the cumulative fraction of the data, of a random distribution of angle differences and of several Gaussian distributions with an average angle difference of  $90^\circ$ . It can be seen from the figure that the data (represented by the solid line) are predominately found close to  $90^\circ$ . The possibility that the data were drawn from a sample of stars where the discs and binary systems are randomly aligned is very small. The KS statistic returns a probability of 1.8% that this is the case. Alternatively, we can reject the models that predict random orientations at the 98.2% confidence level.

We now briefly investigate whether the models predicting aligned discs and binaries can be rejected with equal confidence or not. Although the number of stars under consideration is too small to constrain the specific shape of the underlying distribution, comparing the data with some simple models will give an indication of the nature of the sample. We computed Gaussian distributions with mean angle differ-

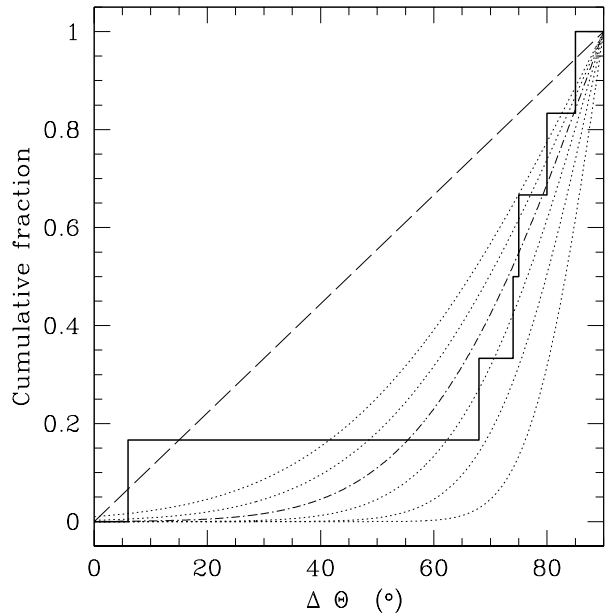


**Figure 7.** The cumulative distribution of the differences between the binary PA and the intrinsic polarization angle. An offset of  $90^\circ$  means that both are aligned (see text). The data, represented by the solid line, are compared with several distributions. The dashed line shows the random distribution, while the dotted lines represent Gaussian distributions with a mean angle difference of  $90^\circ$ , and  $\sigma$  ranging from (from left to right) 35, 30, 25 (indicated by the dashed-dotted line), 20, 15, and  $10^\circ$  respectively. The data are not consistent with a random distribution. If the discs and binaries are assumed to be aligned, the data are well matched by a Gaussian distribution with a width comparable to the observational error.

ences of  $90^\circ$  and  $\sigma$ s ranging from  $35^\circ$  to  $10^\circ$ . The Gaussians were calculated over the range  $0$ - $180^\circ$  and then reprojected to cover  $0$ - $90^\circ$  as we investigate angle *differences*. The results are also shown in Fig. 7. The broadest and narrowest distributions do not match the data at all, but the Gaussians with  $\sigma=20^\circ$  and  $\sigma=25^\circ$ , values close to the experimental error, resemble the data comparatively closely. The KS test returns probabilities of 89% and 93% respectively that the data could be drawn from such a population.

This provides strong evidence in favour of the fragmentation scenario that predicts aligned discs and against the stellar capture scenario which predicts random orientations. A final remark concerns the formation of the more massive stars. The spectral types covered by this sub-sample of objects extends to B0, tracing masses exceeding the maximum possible mass that is accumulated in simple accretion models (e.g. Wolfire & Cassinelli 1987, Bonnell et al. 1998). It appears that the stellar merger scenario which predicts random orientations is also ruled out by our finding.

## 5 CONCLUSIONS

We have studied 31 young stars by means of spectropolarimetry, and find the following.

- (i) A binary frequency of  $68 \pm 11\%$  was found in the

sample of 28 Herbig Ae/Be stars. No other technique has been able to find such a high binary frequency in Herbig Ae/Be stars, demonstrating the proficiency at which spectro-astrometry can detect binaries.

(ii) There is a small hint that the Herbig Be stars are more likely to be found in binaries than the Herbig Ae objects ( $73_{-16}^{+12}\%$  versus  $31_{-14}^{+18}\%$ , the latter rises to  $62_{-17}^{+15}\%$  when the possible detections are included). This could indicate that Herbig Be stars are more likely to be found in binaries than their lower mass Herbig Ae counterparts.

(iii) We detected asymmetric outflows from Z CMa and HD 87643. We conclude that HD 87643 has a high velocity and low velocity outflow, towards the north. No evidence for jets was present in our data.

(iv) We present evidence that the circumprimary discs are aligned with the binary systems. This favours the fragmentation scenario for the formation of Herbig Ae/Be binaries over stellar capture models which predict randomly oriented discs. The next step is to identify the mode of fragmentation, i.e. whether the clouds break up in 2 fragments (predicting roughly fixed mass ratios) or multiple fragments, predicting random mass functions.

(v) The strong alignment, even for early B type stars, provides evidence against the stellar merger scenario invoked to produce massive stars. Instead, as these objects have been found to have discs in the first place, disc accretion remains a viable possibility (cf. Norberg & Maeder 2000).

## ACKNOWLEDGEMENTS

We thank the referee, Rob Jeffries, for his constructive remarks which helped improve the paper. Jorick Vink is thanked for his useful comments on an earlier version of the manuscript. We wish to thank the staff of the Wäldsang in Bakkeveen, where part of this paper was written, for creating an environment making it conducive to study. DB acknowledges support from a student grant from the Particle Physics and Astronomy Research Council of the United Kingdom which also funded MP through a post-doctoral grant. The allocation of time on the Anglo-Australian Telescope was awarded by PATT, the United Kingdom allocation panel. Part of the observations are based on data obtained from the Isaac Newton Telescope, La Palma Spain, in the Spanish Observatorio del Roque de los Muchachos of the Instituto de Astrofísica de Canarias.

## REFERENCES

- Abt H.A., Gomez A.E., Levy S.G. 1990 ApJS 74, 551  
 Bailey J., 1998, MNRAS, 301, 161  
 Bally J., Zinnecker H. 2005, AJ 129, 2281  
 Baines D. Oudmaijer R.D., Mora A. et al., 2004, MNRAS, 353, 697  
 Bertout C. 1989 ARA&A 27, 351  
 Bonnell I.A. & Clarke C.J., 1999, MNRAS, 309, 461  
 Bonnell I.A., Bate M.R., Zinnecker H. 1998, MNRAS 298, 93  
 Bouvier J. & Cororon P., 2001, IAUS 200, 155  
 Cassinelli J.P., Nordsieck K.H., Murison M.A. 1987, ApJ 317, 290  
 Clarke C.J. 2001, IAUS 200, 346  
 Cororon P. & Lagrange A. M., 1999, A&AS, 136, 429  
 Cororon P., 1998, PhD Thesis  
 Dommanget J. & Nys O., 1994, Comm. Obs. R. Belgique, Ser. A, N. 115  
 Drew J.E., Busfield G., Hoare M.G., Murdoch K.A., Nixon C.A., Oudmaijer R.D. 1997, MNRAS 286, 538  
 Duquenois A. & Mayor M., 1991, A&A, 24, 485  
 ESA, 1997, The Hipparcos and Tycho Catalogues, ESA SP-1200  
 Fu H.-H., Hartkopf W.I., Mason B.D., McAlister H.A., Dombrowski E.G., Westin T., Franz O.G. 1997, AJ 114 1623  
 Fukagawa M., Tamura M., Itoh Y., Hayashi S.S., Oasa Y. 2003, ApJ, 590, 49  
 Garcia P.J.V., Thiébaud E., Bacon R., 1999, A&A 346, 892  
 Ghez A. M. Neugebauer G., Matthews K., 1993, AJ, 106, 2005  
 Grady C.A., Polomski E.F., Henning Th. et al., 2001, AJ, 122, 3396  
 Hubrig S., Schöller M., Yudin R.V. 2004, A&A 428, 1  
 Jensen E.L.N., Mathieu R.D., Donar A.X., Dullighan A. 2004, ApJ 600, 789  
 Köhler R. & Leinert C., 1998, 332, 739  
 Koresko C.D., Beckwith S.V.W., Ghez A.M., Matthews K., Neugebauer G. 1991, AJ, 102, 2073  
 Leinert C., Richichi A., Haas M., 1997, A&A, 318, 472  
 Li W. Evans N.J. II, Harvey P.M., Colome C. 1994, ApJ, 433, 199  
 Maheswar G., Manoj P., Bhatt H.C. 2002, A&A 1003  
 Mannings V. & Sargent A. I., 1997, ApJ, 490, 792  
 Mannings V. & Sargent A. I., 2000, ApJ, 529, 391  
 McDonald J.M., Clarke C.J. 1995 MNRAS 275, 671  
 Millan-Gabet R. Schloerb, F.P., Traub W.A. 2001, ApJ, 546, 358  
 Mora A., Merín B., Solano E. et al. 2001, A&A, 378, 116  
 Norberg P., Maeder A. 2000, A&A 359, 1035  
 Oudmaijer R. D. & Drew J. E., 1999, MNRAS, 305, 166  
 Oudmaijer R. D., Proga D., Drew J.E., de Winter D. 1998, MNRAS, 300, 170  
 Piétu V., Dutrey A., Kahane C. 2003, A&A, 398, 565  
 Pirzkal N., Spillar E.J., Dyck H.M., 1997, ApJ, 481, 392  
 Poeckert R., Marlborough J.M. 1976, ApJ 206, 182  
 Poetzel R., Mundt R., Ray T.P. 1989, A&A 224, L13  
 Porter J. M., Oudmaijer R.D., Baines D. 2004, A&A, 428, 327  
 Takami M., Bailey, J. Chrysostomou, A. 2003, A&A 397, 675  
 Testi, L., Palla, F., Natta, A., 1999, A&A, 342, 515  
 Testi L., Palla F., Prusti T., Natta A., Maltagliati S., 1997, A&A, 320, 159  
 Thé P.S., de Winter D., Perez M.R., 1994, A&AS, 104, 315  
 Vink J.S., Drew J.E., Harries T.J., Oudmaijer R.D. 2002, MNRAS, 337, 356  
 Vink J.S., Drew J.E., Harries T.J., Oudmaijer R.D., Unruh Y. 2003, A&A 406, 703  
 Vink J.S., Drew J.E., Harries T.J., Oudmaijer R.D., Unruh Y. 2005, MNRAS, 359, 1049  
 Whelan E.T., Ray T.P., Bacciotti F., Natta A., Testi L., Randich S. 2005, Nature 435, 652  
 Wolf S., Stecklum B., Henning Th. 2001, IAUS 200, 295  
 Wolfire M.G., & Cassinelli J.P. 1987, ApJ 319, 850

## APPENDIX A: SPECTRO-ASTROMETRIC SIMULATIONS OF BINARIES

A spectro-astrometric signature from a binary will arise across a spectroscopic line if there is a difference in intensity from each component star. In the case of  $H\alpha$  emission from a binary system, it is highly unlikely that both components have the same  $H\alpha$  intensities and profiles. Therefore, given the right conditions a spectro-astrometric signature across  $H\alpha$  will be present. Below, with the aid of simulations, we investigate the properties of these signatures.

The approach we use is to simulate the spatial profile at each dispersion pixel, and then build up a 2D spectrum across  $H\alpha$ . The spatial profile from a single star at any particular wavelength can be approximated to a gaussian whose height is in counts (number of photons), and whose width is in spatial pixels (which depends on the seeing and spatial resolution of the instrumental set-up). This is achieved by convolving a point source, where the seeing determines the standard deviation,  $\sigma$ , of the gaussian. In the case of a binary, two point sources at a given separation are convolved. Since the seeing is identical for each star, the widths of the spatial profiles of both components are equal.

The input parameters are the seeing (in arcsecs), the continuum intensity ratios of the primary and secondary,  $I_2/I_1$ , the separation  $d$  (in pixels), the size of the spatial pixels (in arcsec pixel<sup>-1</sup>), and the  $H\alpha$  intensity ratio of the primary and secondary as a function of wavelength,  $H\alpha_2/H\alpha_1$ . In the simplest of binary systems we assume that only one of the stars is emitting  $H\alpha$  and the other has  $H\alpha$  in absorption. Once the spatial profiles have been simulated they are treated as real observations and run through the gaussian fitting program. Both the position and FWHM spectra are then plotted in the usual fashion. Experimental errors are not taken into account in these computations. As an indication of what could be expected, we note that the high signal-to-noise data such as presented here have rms variations on the position and FWHM spectra of order milli-arcseconds. These values are much smaller than the offsets that are discussed here.

In the following sections the effects of changing the input parameters on the spectro-astrometric signatures are investigated. The system under consideration is composed of one star with a broad single peaked  $H\alpha$  emission profile, peaking at 3 times the continuum, and the other star with  $H\alpha$  absorption as broad as the emission profile, and at half the intensity of the continuum. Figure A1 presents the  $H\alpha$  profiles of both components for a separation of 0.5 arcsec, seeing of 1.5 arcsec, and  $I_2/I_1 = 1$ . During the simulations the intensity spectrum of both components is kept fixed, whilst the intensity spectrum of the system (top panel) varies for each simulation, as a function of  $d$ , seeing,  $I_2/I_1$ , and  $H\alpha_2/H\alpha_1$ .

For all of the following simulations, the size of the spatial and dispersion pixels are similar to the instrumental set-up at the AAT in January 2002 ( $\sim 0.15$  arcsec pixel<sup>-1</sup> and  $0.15 \text{ \AA pixel}^{-1}$  ( $6.7 \text{ km s}^{-1} \text{ pixel}^{-1}$ ) respectively, see section 2).

### A1 Changing the separation

Here we change the separation of the binary system whilst all other input parameters are kept constant. A seeing of 1.5 arcsec, representative for the observations discussed in this paper, and continuum intensity ratio,  $I_2/I_1 = 1$ , is chosen. Figure A2a shows the maximum positional and FWHM displacement at  $H\alpha$  from the continuum for several binary separations. For clarity the position and FWHM spectra are centred on zero at the continuum.

As  $d$  increases, the position of the continuum moves away from the  $H\alpha$  emitting star simply because for  $I_2/I_1 = 1$  the continuum is located at  $d/2$ . As we move along  $\lambda$  towards the  $H\alpha$  maximum, the positional displacement moves towards the dominant  $H\alpha$  emitting star. This displacement becomes larger with larger separations.

An increase in the positional displacement as the separation is increased will halt when the spatial profile of the two components becomes fully resolved. This occurs in figure A2a at  $d$  around 3.0 arcsec. At wide separations the technique of spectro-astrometry breaks down because only one profile (in this case the primary star) is fitted by the fitting program at both the continuum and  $H\alpha$  maximum, i.e. spectro-astrometry should only be applied to unresolved binaries. For a separation of 3.0 arcsec the FWHM increases because the spatial profile wings of the primary begin to overlap with the secondary and the fitting program again includes some of the secondary.

For this simulated system a displacement of 0.03 pixels is visible for a separation of only 10 mas. This is a shift of 4.5 mas, which for many of our observed stars is better than the spatial sensitivity, and would therefore be detectable if the observing conditions are similar to, or better than, the simulated parameters. For separations  $< 1.0$  arcsec (the slit width) the positional displacement is larger than the FWHM displacement, at 1.0 arcsec the positional and FWHM displacements are almost identical, and at separations  $> 1.0$  arcsec the positional displacement  $<$  FWHM displacement.

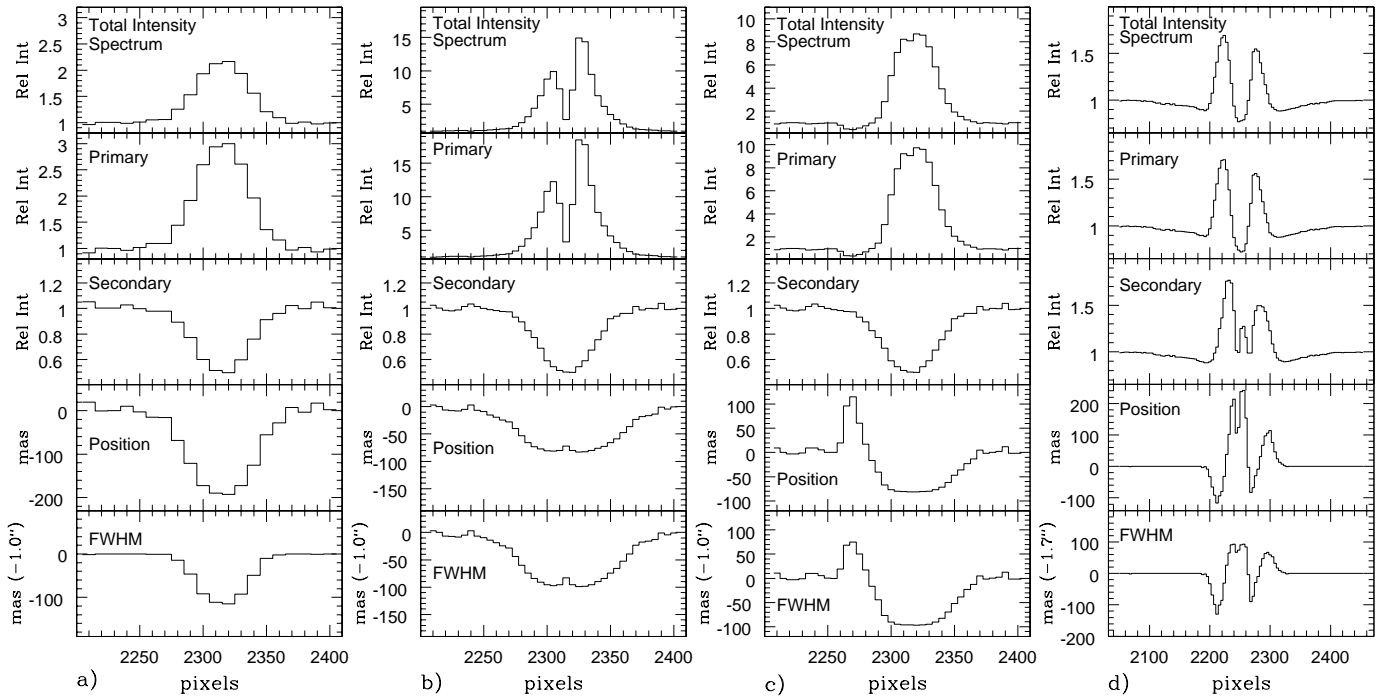
### A2 Changing the seeing

Figure A2b displays the maximum spectro-astrometric displacements for  $d = 1.5$  arcsec,  $I_2/I_1 = 1$ , and varying seeing (from 0.5 to 3.0 arcsec). A decrease in the seeing increases both the positional and FWHM displacement. In this case, for a seeing of 2.0 arcsec and larger, the positional displacement is larger than the FWHM displacement. But for a seeing between 2.0 and 0.5 arcsec the FWHM displacement becomes larger than the positional displacement and the effect of the seeing is rather more significant in the FWHM displacements than in the positional displacements. It is therefore important to approximately know the intrinsic seeing before interpreting the spectro-astrometric signatures, particularly since the seeing can vary considerably between observations. The displacements at a seeing of 0.5 arcsec are zero because the binary is resolved.

### A3 Changing the intensity ratios

Figure A2c show the maximum spectro-astrometric displacements when varying the continuum intensity ratios,  $I_2/I_1$ , whilst keeping the separation (0.5 arcsec) and seeing (1.5





**Figure A1.** Simulated binary systems. a) The primary has H $\alpha$  in emission with a single peaked profile, with seeing = 1.0 arcsec,  $I_2/I_1 = 1.0$ , and  $d = 0.5$  arcsec. b) The primary is emitting H $\alpha$  with a double peaked profile, for seeing = 1.0 arcsec,  $I_2/I_1 = 0.5$ , and  $d = 0.5$  arcsec. c) The primary has a H $\alpha$  P Cygni profile, with seeing = 1.0 arcsec,  $I_2/I_1 = 1/4$ ,  $d = 0.5$  arcsec. d) Both primary and secondary stars are emitting H $\alpha$ . The position and FWHM displacements (lower panels) are similar to those of XY Per observed on 23 Sept 2002 using the binary parameters of the system, seeing = 1.7 arcsec,  $I_2/I_1 = 0.6$ , and  $d = 1.3$  arcsec.

arcsec) constant.  $I_1$  is the H $\alpha$  emitting star, whilst  $I_2$  has H $\alpha$  in absorption. Interestingly, one still sees a positional and FWHM displacement across H $\alpha$ , of 4.5 mas, when the secondary star is a 100th the intensity of the primary star (i.e. a difference of 5 mag). As  $I_2/I_1$  increases to 1, the positional and FWHM displacements increase, and for this separation (0.5 arcsec), the positional displacements increase at larger increments than the FWHM displacements.

At  $I_2/I_1 > 1$  the H $\alpha$  emitter is now the secondary star, and the primary has H $\alpha$  in absorption. As  $I_2/I_1$  increases (from 2 upwards), the positional displacements decrease until no displacement is present, when the H $\alpha$  emitting star is too faint to contribute to the total H $\alpha$  intensity of the system. This is found to occur at  $I_2/I_1 > 300$  for this system. At this point the total H $\alpha$  profile approximates to the H $\alpha$  profile of  $I_2$ . A displacement of 6 mas in both the position and FWHM spectrum, is present when  $I_2/I_1$  is as large as 300 (a difference of  $\sim 6.2$  mag). In this case no H $\alpha$  emission is present in the total intensity spectrum, but the spectro-astrometry still detects the binary.

The FWHM maximum displacements are largest when the primary and secondary star have similar intensities. When the primary is the H $\alpha$  emitter ( $I_2/I_1 \leq 1$ ) the FWHM decreases across H $\alpha$ , whereas when the secondary is the H $\alpha$  emitter the FWHM increases.

#### A4 Changing the H $\alpha$ intensity ratios

Here we investigate the effect of changing the H $\alpha$  intensity ratios,  $H\alpha_2/H\alpha_1$ , whilst the seeing (1.5 arcsec),  $d$  (0.5 arcsec), and  $I_2/I_1$  (1) are kept constant. One component spec-

trum is kept constant, with a single peaked H $\alpha$  emission profile, peaking at 3 times the continuum (identical to the primary spectrum of figure A1a). The other component H $\alpha$  profile is varied.

The results are presented in figure A2d. At  $H\alpha_2/H\alpha_1 = 1$  (and in this case  $I_2/I_1 = 1$ ), the two component H $\alpha$  profiles are identical, therefore we see no displacements in either the position or FWHM spectrum. As the value of  $H\alpha_2/H\alpha_1$  moves further from 1 the positional and FWHM displacements become larger. In the case of the position spectrum, the displacements lie on either side of the position continuum, depending on which star is dominating (i.e. for  $H\alpha_2/H\alpha_1 > 1$ , and  $H\alpha_2/H\alpha_1 < 1$ ). In the case of the FWHM spectrum (bottom panel), any value of  $H\alpha_2/H\alpha_1 \neq 1$  will result in a decrease in the FWHM.

#### A5 Changing the H $\alpha$ profiles

In the above simulations the H $\alpha$  emission profile was kept as a simple single peaked profile. However many Herbig Ae/Be stars have a double peaked or P Cygni H $\alpha$  profile (see for example Reipurth et al., 1996). Figures A1b and c show examples of spectro-astrometric displacements when the primary star of a binary system has a double peaked H $\alpha$  emission profile (from MWC 158) or a P Cygni H $\alpha$  emission profile (from AB Aur). In both cases the secondary star has been chosen to have an H $\alpha$  absorption profile with maximum absorption at 0.5. For figure A1b, the position and FWHM displacements return towards the continuum across the H $\alpha$  minimum because the intensity of the primary diminishes. This produces a 'double peaked' profile in both the posi-

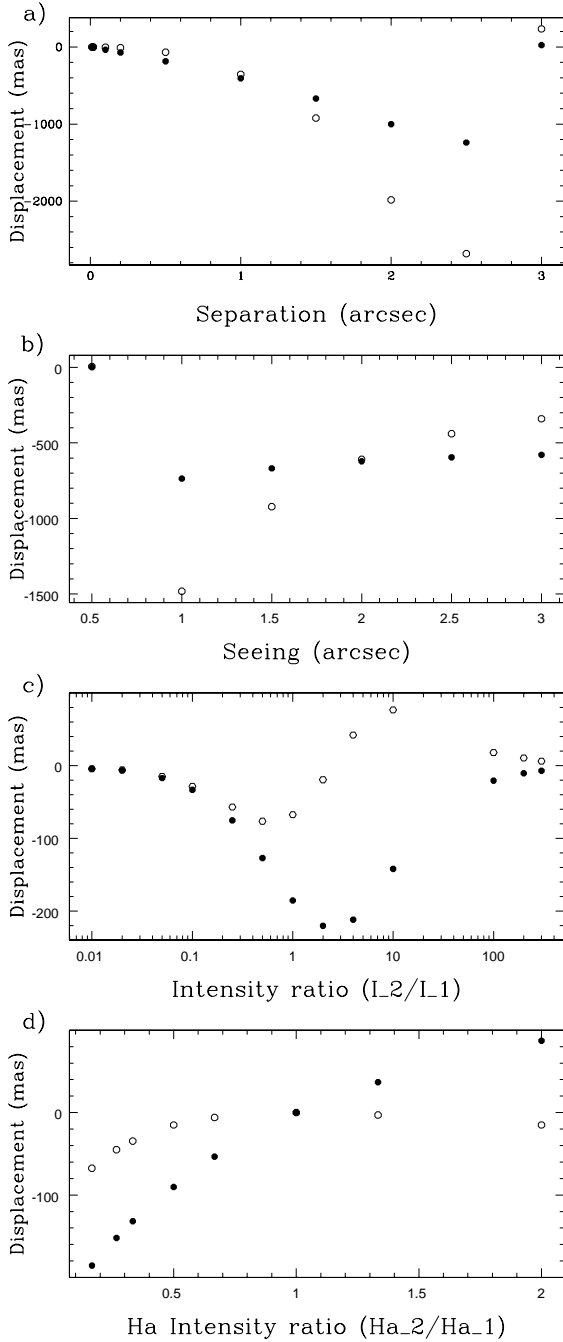


**Figure A2.** The maximum positional displacements (closed circles) and FWHM displacements (open circles) against the parameters binary separation, seeing, binary continuum intensity ratio, and binary  $H\alpha$  intensity ratio. For panel a)  $I_2/I_1 = 1$  and seeing = 1.5 arcsec; panel b)  $I_2/I_1 = 1$  and  $d = 1.5$  arcsec; panel c)  $d = 0.5$  arcsec and seeing = 1.5 arcsec; panel d)  $d = 0.5$  arcsec,  $I_2/I_1 = 1$  and seeing = 1.5 arcsec.

tion and FWHM spectra. The lower panels of figure A1c shows an example of the position and FWHM spectra when the primary has a P Cygni  $H\alpha$  profile. At the peak in the emission we see a typical binary signature, where there is a decrease in the FWHM and a displacement towards the emitting star in the position spectrum. At the P Cygni absorption there is a displacement towards the secondary star

as the intensity of the primary decreases. When  $I_2/I_1 < 1$  the FWHM increases across the P Cygni absorption, again because the intensity of the primary decreases and the secondary becomes more dominant than at the continuum.

In figure A1d both primary and secondary stars are emitting  $H\alpha$ . Since XY Per may be in a system with both components emitting  $H\alpha$  we choose to use binary parameters similar to XY Per, i.e.  $d = 1.3$  arcsec,  $I_2/I_1 = 0.6$ , and seeing = 1.7 arcsec. The positional and FWHM displacements are similar to those of 23rd September 2002 of XY Per in the EW direction. The triple peaked  $H\alpha$  profile of the secondary is not apparent in the total intensity spectrum, but does affect the positional and FWHM displacements.

## A6 Summary

These simulations show how the spectro-astrometric signature from a binary is dependent on the separation of the component stars, the continuum intensity ratio of the two stars, the  $H\alpha$  profiles, and the seeing. The main conclusions from these simulations are: a) the technique is capable of detecting binaries between separations of  $\sim 0.01 - 3.0$  arcsecs, up to a  $\Delta\text{mag}$  of 5 (and as large as  $\Delta\text{mag} = 6$  if the secondary star dominates the  $H\alpha$  emission), for reasonable seeing values ( $\sim 1.5$  arcsec); b) the size of a positional displacement compared with that of a FWHM displacement is an important indication of the binary separation, i.e. binaries with separations approximately  $>$  the slit width will have FWHM displacements as large as, or larger than, the positional displacements. As outlined by Porter et al. (2004), dedicated observations and modelling are needed to retrieve the separation and the individual spectra of both components.